Commun Nonlinear Sci Numer Simulat 146 (2025) 108764

Contents lists available at ScienceDirect

Communications in Nonlinear Science and Numerical Simulation

journal homepage: www.elsevier.com/locate/cnsns

Research paper

Numerical analysis for variable thickness plate with variable order fractional viscoelastic model

Lin Sun [a,b], Jingguo Qu [c,*], Gang Cheng [b], Thierry Barrière [a], Yuhuan Cui [c], Aimin Yang [c], Yiming Chen [d]

[a] Institut FEMTO-ST, National Centre for Scientific Research (CNRS), University of Franche-Comté, 25000 Besancon, France
[b] INSA Centre Val de Loire, Laboratory of Mechanics Gabriel Lamé (LaMé), 41034 Blois, France
[c] College of Science, North China University of Science and Technology, Tangshan, Hebei, 063000, China
[d] School of Science, Yanshan University, Qinhuangdao, Hebei, 066004, China

ARTICLE INFO

Keywords:
Variable thickness viscoelastic plate
Variable order fractional model
Shifted Legendre polynomials
Variable order fractional partial differential equation
Numerical analysis

ABSTRACT

An accurate constitutive model for viscoelastic plates with variable thickness is crucial for understanding their deformation behaviour and optimizing the design of material-based devices. In this study, a variable order fractional model with a precise order function is proposed to effectively characterize the viscoelastic behaviour of variable thickness plates. The shifted Legendre polynomials algorithm is employed to solve the variable order fractional partial differential equation in the time domain, with a minimum absolute error of 1.521×10^{-8}. The computational time is reduced by 30 % and the convergence rate is increased by over 50 % compared to the shifted Bernstein polynomials algorithm. Numerical analysis shows that viscoelastic plates with quadratic thickness variation exhibit the smallest displacement changes and the polyethylene terephthalate plates outperform the polyurethane plates in bending properties. These findings highlight the reliability and effectiveness of the numerical algorithm based on the shifted Legendre polynomials as a powerful tool for solving fractional equations, with significant potential in mechanical engineering.

1. Introduction

Variable thickness plates provide substantial advantages in optimizing material usage and reducing structural weight while maintaining or enhancing its mechanical properties. Compared to uniform thickness plates, these structures are particularly valuable in weight-sensitive and performance-critical applications, such as aerospace, automotive, and civil engineering [1]. In addition to their geometrical advantages, the use of viscoelastic materials further expands their application potential. Gupta and Khanna [2] highlighted that the incorporating both viscoelastic behaviour and thickness variation in structural components not only reduced thier dimensions but also met the rigorous mechanical strength requirements in the aerospace, marine engineering, electronic and optical fields. The vibration characteristics of variable thickness viscoelastic plates under various temperature conditions are important for the applications in the aircraft components, gas turbines, and nuclear power plant structures [3]. It is strongly required to study the bending deformation and damping properties of the viscoelastic plates under different loading conditions. Yu et al. [4] utilized a decoupled wavelet numerical method to analyse the bending deflection of anisotropic viscoelastic plates with variable thickness and discussed the influence of material parameters on the bending stiffness and deformation. Alipour and Shariyat [5]

* Corresponding author.
E-mail address: qujingguo@ncst.edu.cn (J. Qu).

https://doi.org/10.1016/j.cnsns.2025.108764
Received 15 October 2024; Received in revised form 2 February 2025; Accepted 7 March 2025
Available online 17 March 2025

performed a buckling analysis of variable thickness viscoelastic circular plates using Mindlin plate theory. Their results demonstrated that viscoelastic properties significantly delayed the onset of buckling, and the increase of the loss factor resulted in a higher critical buckling load. These findings underscore the critical role of the viscoelasticity in enhancing the structural stability.

It is essential to employ appropriate models that effectively describe the mechanical behaviour of variable thickness viscoelastic plates to better understand the material and structural properties. In Hooke's law, represented by the spring element, the derivative of strain is zero-order, while in Newton's viscosity law, represented by the damping element, the derivative is first-order. A fractional derivative operator with an order between 0 and 1, effectively characterizes the intermediate behaviour between elasticity and viscosity, providing a more comprehensive representation of viscoelastic properties [6]. Fractional derivative operators are increasingly applied in viscoelastic models to improve their accuracy and reduce the number of model parameters. Yu et al. [7] utilized a fractional order (FO) model to describe the three-dimensional viscoelastic behaviour of arterial walls, demonstrating that FO models can accurately represent material properties in a simplified form with fewer parameters. Qing et al. [8] applied the fractional Kelvin-Voigt model to characterize the viscoelasticity of polyethylene terephthalate (PET) membranes. The effects of order function, density coefficient, and various system parameters on the temporal response of PET membranes were elucidated. Variable order fractional (VOF) models, where the fractional derivative varies with time and/or space, have been introduced to provide a more precise representation of the evolution of viscoelastic properties. VOF model has been applied in both theoretical research and practical applications across various fields of science and engineering [9]. Gao et al. [10] employed a VOF model to predict the mechanical behaviour of soft materials, demonstrating improved accuracy and reliability in predicting the compressive stress–strain responses compared to FO models. Meng et al. [11] investigated the performance of VOF viscoelastic models with various order functions. They showed that a linear order function of time effectively described the viscoelastic properties and captured the evolution of mechanical characteristics of the viscoelastic materials. Sun et al. [12] applied VOF model with different forms of order functions to explore the mechanical behaviours of polycarbonate under various temperatures. The efficiency of the proposed VOF model was confirmed based on the experimental data. The VOF model was employed to simulate the mechanical behaviour of the viscoelastic columns. The variations of the displacement under constant, linearly increasing, and simple harmonic loads were investigated [13].

Solving the variable order fractional partial differential equations (VOFPDEs) presents significant challenges due to the complexity introduced by the VOF derivatives. The development of robust numerical methods for solving VOFPDEs is of critical importance. Hassani et al. [14–16] proposed optimization methods employing the generalized polynomials as basis functions to solve VOFPDEs. The solutions were represented as a series expansion of generalized polynomials with unknown coefficients and control parameters. By utilizing the operational matrix and Lagrange multipliers technique, the VOFPDEs were transformed into nonlinear algebraic equations. The effectiveness of the method was rigorously validated through convergence analysis and numerical examples. In contrast to generalized polynomials, orthogonal polynomials satisfy orthogonality conditions with respect to a given weight function. This makes them particularly efficient for solving VOFPDEs. Orthogonal polynomials, such as Legendre [17], Bernoulli [18], Jacobi [19], and Chebyshev [20], not only simplify the computations but also enhance the numerical stability. Hassani et al. [21] introduced transcendental Bernstein series, a generalization of classical Bernstein polynomials, to address variable order space–time fractional equations. These series achieved the same accuracy as Bernstein polynomials with fewer basis functions. A hybrid method combining Bernoulli and Laguerre polynomials was developed to solve VOFPDEs. It exhibits high accuracy with a minimal number of basis functions [22]. Legendre polynomials are particularly useful to solve nonlinear fractional partial differential equations (FPDEs) in physics [23]. Their simplicity and orthogonality with respect to the unit weight function limit the function expansion and optimize the calculation process [24,25]. The numerical algorithm based on Legendre polynomials provide better estimation than that based on Chebyshev polynomials for FPDEs [26]. Legendre polynomials can be extended to shifted Legendre polynomials (SLPs) to better accommodate specific geometric or physical requirements. Cao et al. [27] applied the SLPs algorithm to solve fractional governing equations for poly (methyl methacrylate) (PMMA) beams in the time domain. Sun et al. [28] employed SLPs to solve FO governing equations for viscoelastic plates with uniform thickness. Numerical results highlighted the efficiency, accuracy, and robustness of the algorithm.

This study focuses on employing SLPs to solve VOFPDEs of variable thickness viscoelastic plates. A robust VOF model is proposed to precisely characterize the mechanical behaviour of viscoelastic plate, with the extensive analysis of the order functions to enhance model accuracy. The VOF governing equation incorporates time-varying fractional derivatives and thickness variations that depend on the ordinate variable. The effectiveness and stability of the SLPs algorithm are thoroughly evaluated. The efficiency of the proposed algorithm is validated through the comparisons with the algorithm based on the shifted Bernstein polynomials (SBPs) algorithm. The displacement, stress and bending moment of the plates are investigated in the time domain. These numerical results confirm the high efficiency and accuracy of the proposed SLPs algorithm and demonstrate great application potential.

This paper is structured into six sections. Following the Introduction, Section 2 presents the VOF viscoelastic model, including a detailed explanation of the order function and the formulation of the governing equation for variable thickness viscoelastic plate. Section 3 describes the SLPs approximation method for solving the VOFPDEs. Section 4 provides the theoretical analysis of the SLPs algorithm and evaluates two mathematical examples. In Section 5, numerical analysis of the plate under various conditions is conducted. Finally, Section 6 summarizes the conclusions and outlines perspectives for future research.

2. Material and model

2.1. VOF viscoelastic model with Caputo fractional derivative

Viscoelastic materials exhibit creep, relaxation, and strain-hardening behaviours, which depend not only on the current state of stress and strain but also on their loading history. Fractional derivatives provide the flexibility to describe such nonlocal and

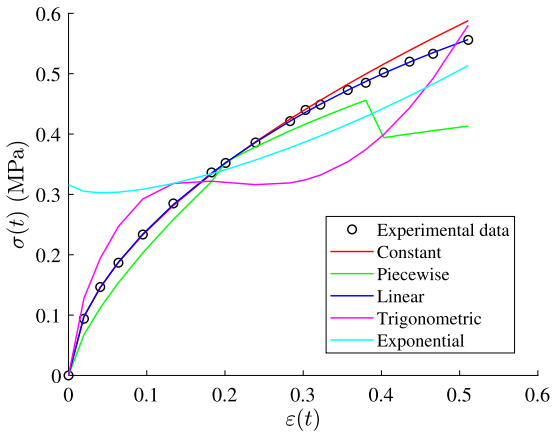

Fig. 1. Comparison of experimental data and predictions by constant FO and VOF models with different order functions.

history-dependent properties by a continuous spectrum of the differentiation orders. The FO viscoelastic model is expressed as [29]:

$$\sigma(t) = E\theta^{\alpha} D_t^{\alpha} \varepsilon(t), 0 \le \alpha < 1, \tag{1}$$

where E is Young's modulus, θ is relaxation time, $D_t^{\alpha}(\cdot)$ represents fractional derivative and α is FO.

The mechanical behaviours of materials are dependent on time, such as creep and stress relaxation under different temperature conditions. Polymers exhibit time-dependent properties near their glass transition temperature [30]. VOF derivatives are introduced to capture these dynamic changes, with the FO α, expressed as a function of time t. The Caputo VOF differential operator is defined as follows [31]:

$$D_t^{\alpha(t)} f(t) = \frac{1}{\Gamma(1-\alpha(t))} \int_{0^+}^{t} (t-s)^{-\alpha(t)} D_s^1 f(s)\, ds, \tag{2}$$

where $\Gamma(*) = \int_0^{\infty} e^{-t} t^{*-1} dt$ is Gamma function.

Substituting the VOF differential operator into Eq. (1), the VOF viscoelastic model is obtained:

$$\sigma(t) = E\theta^{\alpha(t)} D_t^{\alpha(t)} \varepsilon(t), 0 \le \alpha(t) < 1. \tag{3}$$

The properties of Caputo VOF differential operator are as follows [13]:

$$\begin{aligned} &\text{(a) } D_t^{\alpha(t)} G = 0, \\ &\text{(b) } D_t^{\alpha(t)} t^m = \begin{cases} 0, & m = 0, \\ \frac{\Gamma(m+1)}{\Gamma(m+1-\alpha(t))} t^{m-\alpha(t)}, & m = 1, 2, \ldots \end{cases} \\ &\text{(c) } D_t^{\alpha(t)}(G(f(t))) = G D_t^{\alpha(t)} f(t), \end{aligned} \tag{4}$$

where G is constant.

The mechanical properties of polymers change continuously respect to time. This evolution of mechanical behaviour should be intuitively captured by the order function $\alpha(t)$. In prior research by Xiang et al. [32], four types of order functions were evaluated as potential candidates for the VOF model: piecewise, linear, trigonometric, and exponential functions. A comparative analysis revealed that the linear order function was the most efficient due to its simplicity and ability to effectively represent the time-dependent evolution of material properties.

The stress–strain data obtained experimentally was presented in [12]. The VOF models with different order functions are used to fit these experimental results and investigate the impact of the order function. As illustrated in Fig. 1, the constant FO model and VOF model with linear order function are consistent with the stress–strain curve in small strain range. The difference between the experimental data and the numerical model is more important in high strain level for the constant FO model. The VOF model with a linear order function is confirmed to be effective and accurate to capture the stress–strain evolution in the entire strain range.

In this paper, the order function is assumed to be a linear function of time, expressed as:

$$\alpha(t) = at + b, \tag{5}$$

where b represents the initial FO, and a is the rate of change of the FO with respect to time.

2.2. Establishment of VOF governing equation of variable thickness viscoelastic plate

A simply supported-clamped variable thickness viscoelastic plate with a length a and width b is considered, as illustrated in Fig. 2.

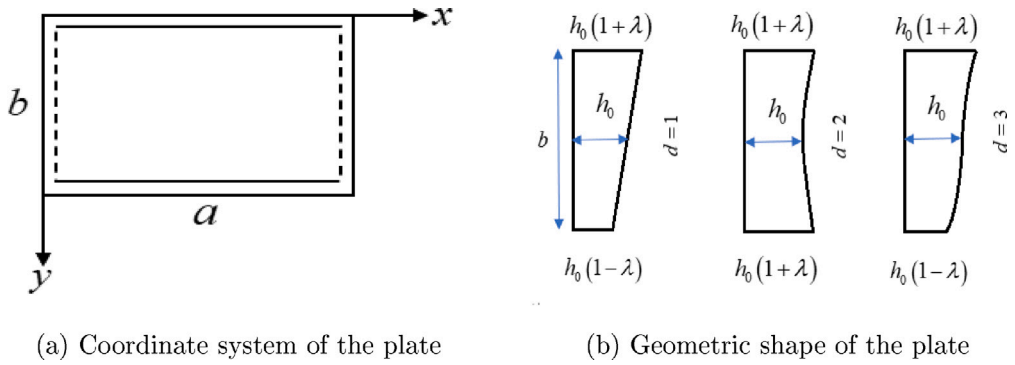

(a) Coordinate system of the plate (b) Geometric shape of the plate

Fig. 2. The schematic of variable thickness viscoelastic plate.

The thickness of this plate is expressed as follows:

$$h(y) = h_0\left[1 + \lambda f_d(y)\right], \tag{6}$$

where h_0 is the reference thickness of the plate, d is the degree of thickness variation function $f_d(y)$ of the plate. λ is a positive constant with a small value. $f_d(y)$ is less than or equal to 1 to make the plate respect the classical thin plate theory. The form of $f_d(y)$ is as follows:

$$f_d(y) = \left(\frac{2y}{b} - 1\right)^d, \quad d = 1, 2, 3, \ldots \tag{7}$$

$u(x, y, t)$ is supposed to be the transverse vibration displacement of the plate, x and y are transverse and axial coordinate respectively, t is time.

The bending strain of the thin plate, including the components in the x-direction, y-direction and shear direction, expressed as follows:

$$\begin{aligned}
\varepsilon_x &= \frac{\partial u_x}{\partial x}, \\
\varepsilon_y &= \frac{\partial u_y}{\partial y}, \\
\gamma_{xy} &= \frac{\partial u_x}{\partial y} + \frac{\partial u_y}{\partial x}.
\end{aligned} \tag{8}$$

The bending strain can be calculated by the transverse displacement $u(x, y, t)$.

$$\begin{aligned}
u_x &= -z\frac{\partial u}{\partial x}, \\
u_y &= -z\frac{\partial u}{\partial y},
\end{aligned} \tag{9}$$

where z is the distance from the mid-plane of the plate.

The relationship between the bending strain components and transverse displacement is:

$$\begin{aligned}
\varepsilon_x &= \frac{\partial u_x}{\partial x} = \frac{\partial}{\partial x}\left(-z\frac{\partial u}{\partial x}\right) = -z\frac{\partial^2 u}{\partial x^2}, \\
\varepsilon_y &= \frac{\partial u_y}{\partial y} = \frac{\partial}{\partial y}\left(-z\frac{\partial u}{\partial y}\right) = -z\frac{\partial^2 u}{\partial y^2}, \\
\gamma_{xy} &= \frac{\partial u_x}{\partial y} + \frac{\partial u_y}{\partial x} = \frac{\partial}{\partial y}\left(-z\frac{\partial u}{\partial x}\right) + \frac{\partial}{\partial x}\left(-z\frac{\partial u}{\partial y}\right) = -2z\frac{\partial^2 u}{\partial x \partial y}.
\end{aligned} \tag{10}$$

Based on the theory of linear elasticity, the constitutive relation between the stress and strain of the plate is expressed as follows [33]:

$$\begin{Bmatrix} \sigma_x \\ \sigma_y \\ \tau_{xy} \end{Bmatrix} = \frac{E}{\left(1-\nu^2\right)} \begin{bmatrix} 1 & \nu & 0 \\ \nu & 1 & 0 \\ 0 & 0 & \left(\frac{1-\nu}{2}\right) \end{bmatrix} \begin{Bmatrix} \varepsilon_x \\ \varepsilon_y \\ \gamma_{xy} \end{Bmatrix}, \tag{11}$$

where σ_x and σ_y represent the normal stresses and τ_{xy} represents the shear stress, ν is Poisson's ratio.

Viscoelastic materials exhibit time-dependent behaviour, meaning that their stress response depends not only on the current strain but also on the strain history. The VOF derivative $D_t^{\alpha(t)}$ is incorporated in the stress–strain relation to capture the viscoelastic

material's memory effects and time-dependent behaviour. The term $\theta^{\alpha(t)}$ is also added to describe the evolution of viscoelastic behaviour.

Based on Eq. (11) and VOF model (Eq. (3)), the stresses can be expressed as follows [34]:

$$\begin{aligned}
\sigma_x &= \frac{E\theta^{\alpha(t)} D_t^{\alpha(t)}}{1-\nu^2}\left(\varepsilon_x + \nu\varepsilon_y\right),\\
\sigma_y &= \frac{E\theta^{\alpha(t)} D_t^{\alpha(t)}}{1-\nu^2}\left(\varepsilon_y + \nu\varepsilon_x\right),\\
\tau_{xy} &= \frac{E\theta^{\alpha(t)} D_t^{\alpha(t)}}{2\left(1-\nu^2\right)}(1-\nu)\gamma_{xy},
\end{aligned} \tag{12}$$

At each unit width of the cross-section of the variable thickness plate, σ_x, σ_y and τ_{xy} are respectively combined into bending moments M_x, M_y and twisting moment M_{xy}, which are as follows:

$$\begin{aligned}
M_x &= \int_{-\frac{h(y)}{2}}^{\frac{h(y)}{2}} z\sigma_x dz = -D(y)\left(\frac{\partial^2 u}{\partial x^2} + \nu\frac{\partial^2 u}{\partial y^2}\right),\\
M_y &= \int_{-\frac{h(y)}{2}}^{\frac{h(y)}{2}} z\sigma_y dz = -D(y)\left(\frac{\partial^2 u}{\partial y^2} + \nu\frac{\partial^2 u}{\partial x^2}\right),\\
M_{xy} &= \int_{-\frac{h(y)}{2}}^{\frac{h(y)}{2}} z\tau_{xy} dz = -D(y)(1-\nu)\frac{\partial^2 u}{\partial x\partial y},
\end{aligned} \tag{13}$$

where $D(y) = D_0\left[1+\lambda f_d(y)\right]^3$, $D_0 = \frac{Eh_0^3\theta^{\alpha(t)}D_t^{\alpha(t)}}{12(1-\nu^2)}$.

When a distributed load $F(x,y,t)$ is imposed on the upper surface of variable thickness plate, its governing equation is written as [34] :

$$\frac{\partial^2 M_x}{\partial x^2} + 2\frac{\partial^2 M_{xy}}{\partial x\partial y} + \frac{\partial^2 M_y}{\partial y^2} + \rho h(y)\frac{\partial^2 u(x,y,t)}{\partial t^2} = F(x,y,t), \tag{14}$$

where ρ is density of plate.

Based on Eqs. (13) and (14), the VOF governing equation of variable thickness viscoelastic plate is:

$$-\frac{Eh(y)^3\theta^{\alpha(t)}D_t^{\alpha(t)}}{12\left(1-\nu^2\right)}\left(\frac{\partial^4 u(x,y,t)}{\partial x^4} + 2\frac{\partial^4 u(x,y,t)}{\partial x^2\partial y^2} + \frac{\partial^4 u(x,y,t)}{\partial y^4}\right) + \rho h(y)\frac{\partial^2 u(x,y,t)}{\partial t^2} = F(x,y,t). \tag{15}$$

The initial conditions are given by:

$$u(x,y,0) = \left.\frac{\partial u(x,y,t)}{\partial t}\right|_{t=0} = 0. \tag{16}$$

The boundary conditions are determined by:

$$u(x,y,t)|_{x=0,a} = u(x,y,t)|_{y=0,b} = \left.\frac{\partial u(x,y,t)}{\partial y}\right|_{y=0,b} = \left.\frac{\partial^2 u(x,y,t)}{\partial x^2}\right|_{x=0,a} = 0. \tag{17}$$

3. SLPs algorithm for solving VOFPDEs

3.1. Properties of SLPs

SLPs $l_m(x)$ are derived from the standard Legendre polynomials $l_m^*(x)$ by shifting their domain from [−1,1] to [0,1]:

$$l_m(x) = l_m^*(x)(2x-1), \tag{18}$$

where m is the degree of the polynomials.

The definition of SLPs is [35],

$$l_m(x) = \sum_{p=0}^{m}(-1)^{m+p}\frac{\Gamma(m+p+1)}{\Gamma(m-p+1)(\Gamma(p+1))^2}x^p, \tag{19}$$

where $p = 0, 1, \ldots, m$.

SLPs possess the following orthogonal property [36]:

$$\int_0^1 l_p(x)l_q(x)dx = \begin{cases}\frac{1}{2p+1}, & p=q,\\ 0, & p\neq q,\end{cases} \tag{20}$$

where $p, q = 0, 1, \ldots, m$.

$\boldsymbol{\Phi}_m(x)$ is represented as a vector form consisting of a series of SLPs,

$$\boldsymbol{\Phi}_m(x) = \left[l_p(x), 0 \le p \le m\right]^T. \tag{21}$$

It can be transformed as:

$$\boldsymbol{\Phi}_m(x) = GA(x), \tag{22}$$

where $A(x) = [1, x, \dots, x^m]^T$,

$$G = \left[g_{pq}\right]_{p,q=0}^{m},\ \left[g_{pq}\right] = \begin{cases} (-1)^{p+q}\frac{\Gamma(p+q+1)}{\Gamma(p-q+1)(\Gamma(p+1))^2}, & p \ge q, \\ 0, & p < q. \end{cases} \tag{23}$$

SLPs are extended to the interval $[0, R]$ to be more suitable for practical application. SLPs of degree m_1 can be obtained.

$$\begin{aligned} L_{m_1}(x) &= \sum_{p=0}^{m_1} (-1)^{m_1+p} \frac{\Gamma(m_1+p+1)}{\Gamma(m_1-p+1)(\Gamma(p+1))^2} \left(\frac{x}{R}\right)^p \\ &= \sum_{p=0}^{m_1} (-1)^{m_1+p} \frac{\Gamma(m_1+p+1)}{\Gamma(m_1-p+1)(\Gamma(p+1))^2} \left(\frac{1}{R}\right)^p x^p, \end{aligned}$$

where $x \in [0, R],\ p = 0, 1, \dots, m_1$.

$\boldsymbol{\Phi}_{m_1}(x)$ is expressed as:

$$\boldsymbol{\Phi}_{m_1}(x) = SP(x), \tag{24}$$

where $P(x) = [1, x, \dots, x^{m_1}]^T$,

$$S = [s_{pq}]_{p,q=0}^{m_1},\ \left[s_{pq}\right] = \begin{cases} (-1)^{p+q}\frac{\Gamma(p+q+1)}{\Gamma(p-q+1)(\Gamma(p+1))^2}\left(\frac{1}{R}\right)^p, & p \ge q, \\ 0, & p < q. \end{cases} \tag{25}$$

By using the same approximation method, $\boldsymbol{\Phi}_{m_2}(y)$ is expressed in the following form:

$$\boldsymbol{\Phi}_{m_2}(y) = KP(y), \tag{26}$$

where $y \in [0, N]$, $P(y) = [1, y, \dots, y^{m_2}]^T$.

$$K = [k_{pq}]_{p,q=0}^{m_2},\ \left[k_{pq}\right] = \begin{cases} (-1)^{p+q}\frac{\Gamma(p+q+1)}{\Gamma(p-q+1)(\Gamma(p+1))^2}\left(\frac{1}{N}\right)^p, & p \ge q, \\ 0, & p < q. \end{cases} \tag{27}$$

$\boldsymbol{\Phi}_{m_3}(t)$ is expressed in the following form:

$$\boldsymbol{\Phi}_{m_3}(t) = HP(t), \tag{28}$$

where $t \in [0, M]$, $P(t) = [1, t, \dots, t^{m_3}]^T$.

$$H = [h_{pq}]_{p,q=0}^{m_3},\ \left[h_{pq}\right] = \begin{cases} (-1)^{p+q}\frac{\Gamma(p+q+1)}{\Gamma(p-q+1)(\Gamma(p+1))^2}\left(\frac{1}{M}\right)^p, & p \ge q, \\ 0, & p < q. \end{cases} \tag{29}$$

3.2. Approximation of unknown function by SLPs

The analytical solution of $u(x, y, t)$ is impossible to obtain directly by the symbolic manipulation. It is expressed as a product of two independent functions to approximate its analytical solution: one is dependent on the spatial variables $u(x, y)$, and the other is on the temporal variable $u(t)$ [34].

$$u(x, y, t) = u(x, y)u(t), \tag{30}$$

where $u(x, y) \in L^2([0, R] \times [0, N]), u(t) \in L^2([0, M])$.

$u(t) \in L^2([0, M])$ is approximated by SLPs as finite terms,

$$u(t) \approx \sum_{k=0}^{m_3} c_k L_k(t) = C^T \boldsymbol{\Phi}_{m_3}(t), \tag{31}$$

where m_3 is the number of terms of SLPs, $\boldsymbol{\Phi}_{m_3}(t) = \left[L_k(t), 0 \le k \le m_3\right]^T$. $C^T = \left[c_k\right]_{k=0}^{m_3}$ is an unknow coefficient matrix as following:

$$C^T \left\langle \boldsymbol{\Phi}_{m_3}(t), \boldsymbol{\Phi}_{m_3}^T(t) \right\rangle = \left\langle u(t), \boldsymbol{\Phi}_{m_3}^T(t) \right\rangle. \tag{32}$$

Then,

$$C^T = \left\langle u(t), \boldsymbol{\Phi}_{m_3}^T(t) \right\rangle \Theta^{-1}, \tag{33}$$

where $\Theta = \left\langle \boldsymbol{\Phi}_{m_3}(t), \boldsymbol{\Phi}_{m_3}^T(t) \right\rangle = \left[\vartheta_{kl}\right]_{k,l=0}^{m_3}$,

$$\vartheta_{kl} = \int_0^M L_{m_3,k}(t) L_{m_3,l}(t) dt = \begin{cases} 0, & k \neq l, \\ \frac{M}{k+l+1}, & k = l, \end{cases} (k, l = 0, 1, \ldots, m_3). \tag{34}$$

$u(x, y) \in L^2([0, R] \times [0, N])$ is approximated,

$$u(x, y) \approx \sum_{p=0}^{m_1} \sum_{q=0}^{m_2} u_{pq} L_p(x) L_q(y) = \boldsymbol{\Phi}_{m_1}^T(x) U \boldsymbol{\Phi}_{m_2}(y), \tag{35}$$

where m_1, m_2 is the number of terms of SLPs, $\boldsymbol{\Phi}_{m_1}(x) = \left[L_p(x), 0 \le p \le m_1\right]^T$, $\boldsymbol{\Phi}_{m_2}(y) = \left[L_q(y), 0 \le q \le m_2\right]^T$. $U = \begin{bmatrix} u_{0,0} & u_{0,1} & \cdots & u_{0,m_2} \\ u_{1,0} & u_{1,1} & \cdots & u_{1,m_2} \\ \vdots & \vdots & \ddots & \vdots \\ u_{m_1,0} & u_{m_1,1} & \cdots & u_{m_1,m_2} \end{bmatrix}$ is the $(m_1 + 1) \times (m_2 + 1)$ order coefficient matrix that needs to be identified.

Eqs. (31) and (35) are substituted to Eq. (30) to obtain the following equation:

$$u(x, y, t) \approx \boldsymbol{\Phi}_{m_1}^T(x) U \boldsymbol{\Phi}_{m_2}(y) C^T \boldsymbol{\Phi}_{m_3}(t). \tag{36}$$

3.3. Operator matrices

3.3.1. Integer order differential operator matrices

The first-order derivative of $\boldsymbol{\Phi}_{m_1}$ is written as $D_x \boldsymbol{\Phi}_{m_1}(x)$, according to Eq. (24), it can be transformed as:

$$D_x \boldsymbol{\Phi}_{m_1}(x) = (SP(x))' = S \begin{bmatrix} 0 \\ 1 \\ \vdots \\ m_1 x^{m_1 - 1} \end{bmatrix} = S V_1 P(x), \tag{37}$$

where $V_1 = [v_{pq}]_{p,q=0}^{m_1}$, $v_{pq} = \begin{cases} 0, & p \neq q + 1, \\ i, & p = q + 1. \end{cases}$

According to Eqs. (24) and (37), $D_x \boldsymbol{\Phi}_{m_1}(x)$ can be rewritten as follows:

$$D_x \boldsymbol{\Phi}_{m_1}(x) = S V_1 S^{-1} \boldsymbol{\Phi}_{m_1}(x), \tag{38}$$

where $D_x = S V_1 S^{-1}$ is considered as a first-order differential operator matrix of the SLPs.

Similarly,

$$D_x^2 \boldsymbol{\Phi}_{m_1}(x) = (\boldsymbol{\Phi}'_{m_1}(x))' = S V_1 S^{-1} \boldsymbol{\Phi}'_{m_1}(x) = (S V_1 S^{-1})^2 \boldsymbol{\Phi}_{m_1}(x), \tag{39}$$

where $D_x^2 = (S V_1 S^{-1})^2$ is considered as a second-order differential operator matrix of the SLPs.

In conclusion, the n-order differential operator matrices for SLPs are obtained.

$$D_x^n \boldsymbol{\Phi}_{m_1}(x) = (S V_1 S^{-1})^n \boldsymbol{\Phi}_{m_1}(x), \tag{40}$$

$$D_y^n \boldsymbol{\Phi}_{m_2}(y) = (K V_2 K^{-1})^n \boldsymbol{\Phi}_{m_2}(y), \tag{41}$$

$$D_t^n \boldsymbol{\Phi}_{m_3}(t) = (H V_3 H^{-1})^n \boldsymbol{\Phi}_{m_3}(t), \tag{42}$$

where $V_2 = [v_{pq}]_{p,q=0}^{m_2}$, $V_3 = [v_{pq}]_{p,q=0}^{m_3}$.

The integer order derivative terms in Eq. (15) are rewritten as:

$$\frac{\partial^4 u(x, y, t)}{\partial x^4} \approx \boldsymbol{\Phi}_{m_1}^T(x) \left(S V_1 S^{-1}\right)^4 U \boldsymbol{\Phi}_{m_2}(y) C^T \boldsymbol{\Phi}_{m_3}(t), \tag{43}$$

$$\frac{\partial^4 u(x, y, t)}{\partial y^4} \approx \boldsymbol{\Phi}_{m_1}^T(x) U \left(K V_2 K^{-1}\right)^4 \boldsymbol{\Phi}_{m_2}(y) C^T \boldsymbol{\Phi}_{m_3}(t), \tag{44}$$

$$\frac{\partial^4 u(x, y, t)}{\partial x^2 \partial y^2} \approx \boldsymbol{\Phi}_{m_1}^T(x) \left(S V_1 S^{-1}\right)^2 U \left(K V_2 K^{-1}\right)^2 \boldsymbol{\Phi}_{m_2}(y) C^T \boldsymbol{\Phi}_{m_3}(t), \tag{45}$$

$$\frac{\partial^2 u(x, y, t)}{\partial t^2} \approx \boldsymbol{\Phi}_{m_1}^T(x) U \boldsymbol{\Phi}_{m_2}(y) C^T \left(H V_3 H^{-1}\right)^2 \boldsymbol{\Phi}_{m_3}(t). \tag{46}$$

3.3.2. VOF differential operator matrices

The $\alpha(t)$ differential operator of t_{m_3} is expressed by using the definition of VOF derivative,

$$D_t^{\alpha(t)} t^{m_3} = \frac{\Gamma(m_3+1)}{\Gamma(m_3+1-\alpha(t))} t^{m_3-\alpha(t)}. \tag{47}$$

VOF derivative of $\boldsymbol{\Phi}_{m_3}(t)$ is obtained according to Eqs. (28) and (47),

$$D_t^{\alpha(t)} \boldsymbol{\Phi}_{m_3}(t) = D_t^{\alpha(t)}(HP(t)) = H \begin{bmatrix} 0 \\ \frac{\Gamma(2)}{\Gamma(2-\alpha(t))} t^{1-\alpha(t)} \\ \vdots \\ \frac{\Gamma(m_3+1)}{\Gamma(m_3+1-\alpha(t))} t^{m_3-\alpha(t)} \end{bmatrix} = HJP(t), \tag{48}$$

where $J = \left[j_{pq}\right]_{p,q=0}^{m_3}$, $j_{pq} = \begin{cases} 0, & \text{otherwise}, \\ \frac{\Gamma(p)}{\Gamma(p+1-\alpha(t))} t^{-\alpha(t)}, & p = q, p \neq 1. \end{cases}$

According to Eq. (28), Eq. (48) is rewritten as:

$$D_t^{\alpha(t)} \boldsymbol{\Phi}_{m_3}(t) = HJH^{-1} \boldsymbol{\Phi}_{m_3}(t) = K_t \boldsymbol{\Phi}_{m_3}(t), \tag{49}$$

where K_t=HJH^{-1} is the VOF differential operator matrix of $\boldsymbol{\Phi}_{m_3}(t)$.

VOF derivatives terms in Eq. (15) are rewritten as:

$$D_t^{\alpha(t)} \frac{\partial^4 u(x,y,t)}{\partial x^4} \approx \boldsymbol{\Phi}_{m_1}^T(x) \left(SV_1S^{-1}\right)^4 U \boldsymbol{\Phi}_{m_2}(y) C^T HJH^{-1} \boldsymbol{\Phi}_{m_3}(t), \tag{50}$$

$$D_t^{\alpha(t)} \frac{\partial^4 u(x,y,t)}{\partial y^4} \approx \boldsymbol{\Phi}_{m_1}^T(x) U \left(KV_2K^{-1}\right)^4 \boldsymbol{\Phi}_{m_2}(y) C^T HJH^{-1} \boldsymbol{\Phi}_{m_3}(t), \tag{51}$$

$$D_t^{\alpha(t)} \frac{\partial^4 u(x,y,t)}{\partial x^2 \partial y^2} \approx \boldsymbol{\Phi}_{m_1}^T(x) \left(SV_1S^{-1}\right)^2 U \left(KV_2K^{-1}\right)^2 \boldsymbol{\Phi}_{m_2}(y) C^T HJH^{-1} \boldsymbol{\Phi}_{m_3}(t). \tag{52}$$

Based on Eqs. (46), (50), (51) and (52), the governing equation Eq. (15) is rewritten as follows:

$$\begin{aligned} &-\frac{Eh(y)^3 \theta^{\alpha(t)} D_t^{\alpha(t)}}{12\left(1-\nu^2\right)} \boldsymbol{\Phi}_{m_1}^T(x) \left(SV_1S^{-1}\right)^4 U \boldsymbol{\Phi}_{m_2}(y) C^T HJH^{-1} \boldsymbol{\Phi}_{m_3}(t) \\ &-\frac{Eh(y)^3 \theta^{\alpha(t)} D_t^{\alpha(t)}}{12\left(1-\nu^2\right)} \boldsymbol{\Phi}_{m_1}^T(x) \left(SV_1S^{-1}\right)^2 U \left(KV_2K^{-1}\right)^2 \boldsymbol{\Phi}_{m_2}(y) C^T HJH^{-1} \boldsymbol{\Phi}_{m_3}(t) \\ &-\frac{Eh(y)^3 \theta^{\alpha(t)} D_t^{\alpha(t)}}{12\left(1-\nu^2\right)} \boldsymbol{\Phi}_{m_1}^T(x) U \left(KV_2K^{-1}\right)^4 \boldsymbol{\Phi}_{m_2}(y) C^T HJH^{-1} \boldsymbol{\Phi}_{m_3}(t) \\ &+\rho h(y) \boldsymbol{\Phi}_{m_1}^T(x) U \boldsymbol{\Phi}_{m_2}(y) C^T \left(HV_3H^{-1}\right)^2 \boldsymbol{\Phi}_{m_3}(t) = F(x,y,t), \end{aligned} \tag{53}$$

The initial and boundary conditions are approximated as:

$$\begin{aligned} &u(x,y,0) \approx \boldsymbol{\Phi}_{m_1}^T(x) U \boldsymbol{\Phi}_{m_2}(y) C^T \boldsymbol{\Phi}_{m_3}(0) = 0, \\ &\frac{\partial u(x,y,0)}{\partial t} \approx \boldsymbol{\Phi}_{m_1}^T(x) U \boldsymbol{\Phi}_{m_2}(y) C^T \left(HV_3H^{-1}\right) \boldsymbol{\Phi}_{m_3}(0) = 0, \\ &u(0,y,t) \approx \boldsymbol{\Phi}_{m_1}^T(0) U \boldsymbol{\Phi}_{m_2}(y) C^T \boldsymbol{\Phi}_{m_3}(t) = 0, \\ &u(a,y,t) \approx \boldsymbol{\Phi}_{m_1}^T(a) U \boldsymbol{\Phi}_{m_2}(y) C^T \boldsymbol{\Phi}_{m_3}(t) = 0, \\ &u(x,0,t) \approx \boldsymbol{\Phi}_{m_1}^T(x) U \boldsymbol{\Phi}_{m_2}(0) C^T \boldsymbol{\Phi}_{m_3}(t) = 0, \\ &u(x,b,t) \approx \boldsymbol{\Phi}_{m_1}^T(x) U \boldsymbol{\Phi}_{m_2}(b) C^T \boldsymbol{\Phi}_{m_3}(t) = 0, \\ &\frac{\partial u(x,0,t)}{\partial y} \approx \boldsymbol{\Phi}_{m_1}^T(x) U K V_2 K^{-1} \boldsymbol{\Phi}_{m_2}(0) C^T \boldsymbol{\Phi}_{m_3}(t) = 0, \\ &\frac{\partial u(x,b,t)}{\partial y} \approx \boldsymbol{\Phi}_{m_1}^T(x) U K V_2 K^{-1} \boldsymbol{\Phi}_{m_2}(b) C^T \boldsymbol{\Phi}_{m_3}(t) = 0, \\ &\frac{\partial^2 u(0,y,t)}{\partial x^2} \approx \boldsymbol{\Phi}_{m_1}^T(0) \left(SV_1S^{-1}\right)^2 U \boldsymbol{\Phi}_{m_2}(y) C^T \boldsymbol{\Phi}_{m_3}(t) = 0, \\ &\frac{\partial^2 u(a,y,t)}{\partial x^2} \approx \boldsymbol{\Phi}_{m_1}^T(a) \left(SV_1S^{-1}\right)^2 U \boldsymbol{\Phi}_{m_2}(y) C^T \boldsymbol{\Phi}_{m_3}(t) = 0. \end{aligned} \tag{54}$$

$u(x,y,t)$ is discretized into $u(x_i,y_j,t_k)$ by applying the collocation method to solve these equations [37]. The three variables are discretized as follows:

$$x_i = \frac{2i-1}{2\left(m_1+1\right)} R, i = 0,1,2,\ldots,m_1,$$

$$y_j = \frac{2j-1}{2\left(m_2+1\right)}N, j = 0, 1, 2, \ldots, m_2,$$
$$t_k = \frac{2k-1}{2\left(m_3+1\right)}M, k = 0, 1, 2, \ldots, m_3. \tag{55}$$

These equations indicate that m_1+1, m_2+1, m_3+1 nodes are selected in a given interval $[0, R], [0, N], [0, M]$. The collection node is selected at the centre of each interval to avoid the boundary point. Eq. (53) is converted into a series of algebraic equations. The unknown coefficient matrices U and C in the equation are solved by the least squares method. U and C are substituted back into the Eq. (36) to obtain the numerical solution $u(x, y, t)$ in the time domain. The entire process is implemented in MATLAB R2017b on a laptop with a 1.60 GHz processor and 4 GB random access memory. The numerical results demonstrated the SLPs algorithm has high computational efficiency, the computation time is around 20 s.

The implementation of the SLPs algorithm is summarized as:

Algorithm 1 Numerical solution for the VOFPDEs based on SLPs algorithm

Input: $E, \alpha(t), \theta, \nu, \rho, h(y), F(x, y, t)$
Output: $u(x, y, t)$

1. Function approximation based on SLPs algorithm: $u(x, y, t) \approx \boldsymbol{\Phi}_{m_1}^T(x) U \boldsymbol{\Phi}_{m_2}(y) C^T \boldsymbol{\Phi}_{m_3}(t)$
2. Derivative calculations of integer order and VOF differential operator matrices
3. Substitution of the operator matrices into the initial governing equation
4. Discretization of the variables: $x_i = \frac{2i-1}{2(m_1+1)}R, i = 0, 1, 2, \cdots m_1$; $y_j = \frac{2j-1}{2(m_2+1)}N, j = 0, 1, 2, \cdots, m_2$; $t_k = \frac{2k-1}{2(m_3+1)}M, k = 0, 1, 2, \cdots, m_3$ for transforming the governing equation into the algebraic equations
5. Solving the algebraic equations based on the least squares method by using MATLAB

4. Theoretical analysis and mathematical examples

In this section, the error estimation, convergence analysis and stability analysis for the proposed method are discussed.

4.1. Error estimation

$u_{m_1,m_2,m_3}(x, y, t)$ is assumed as the best approximation of a continuous function $u(x, y, t) \in \Omega$, where $\Omega = [0, R] \times [0, N] \times [0, M]$, in the space of $m_1 \times m_2 \times m_3$ terms SLPs $\Xi_{m_1,m_2,m_3}(x, y, t)$. Any polynomial $v_{m_1,m_2,m_3}(x, y, t)$ in variables x, y and t follows that:

$$\left\| u(x, y, t) - u_{m_1,m_2,m_3}(x, y, t) \right\|_2 \le \left\| u(x, y, t) - v_{m_1,m_2,m_3}(x, y, t) \right\|_2, \tag{56}$$

$v_{m_1,m_2,m_3}(x, y, t)$ is the interpolating polynomial of u at nodes (x_i, y_j, t_k), $x_i = i\frac{R}{m_1}$, $y_j = j\frac{N}{m_2}$, $t_k = k\frac{M}{m_3}$,

$$\begin{aligned} & u(x, y, t) - v_{m_1,m_2,m_3}(x, y, t) \\ &= \frac{\partial^{m_1+1}}{\partial x^{m_1+1}} u(\xi, y, t) A_1 + \frac{\partial^{m_2+1}}{\partial y^{m_2+1}} u(x, \sigma, t) A_2 + \frac{\partial^{m_3+1}}{\partial t^{m_3+1}} u(x, y, \omega) A_3 \\ &- \frac{\partial^{m_1+m_2+m_3+3}}{\partial x^{m_1+1} \partial y^{m_2+1} \partial t^{m_3+1}} u\left(\xi', \sigma', \omega'\right) A_1 A_2 A_3, \end{aligned} \tag{57}$$

where $\xi, \xi' \in [0, R], \sigma, \sigma' \in [0, N]$ and $\omega, \omega' \in [0, M]$. $A_1 = \prod_{i=0}^{m_1}(x - x_i), A_2 = \prod_{j=0}^{m_2}(y - y_j)$ and $A_3 = \prod_{k=0}^{m_3}(t - t_k)$. It can be obtained:

$$\begin{aligned} & \left| u(x, y, t) - v_{m_1,m_2,m_3}(x, y, t) \right| \\ & \le \max_{(x,y,t)\in\Omega} \left| \frac{\partial^{m_1+1} u(x, y, t)}{\partial x^{m_1+1}\left(m_1+1\right)!} \right| A_1 \\ & + \max_{(x,y,t)\in\Omega} \left| \frac{\partial^{m_2+1} u(x, y, t)}{\partial y^{m_2+1}\left(m_2+1\right)!} \right| A_2 \\ & + \max_{(x,y,t)\in\Omega} \left| \frac{\partial^{m_3+1} u(x, y, t)}{\partial t^{m_3+1}\left(m_3+1\right)!} \right| A_3 \\ & - \max_{(x,y,t)\in\Omega} \left| \frac{\partial^{m_1+m_2+m_3+3} u(x, y, t)}{\partial x^{m_1+1} \partial y^{m_2+1} \partial t^{m_3+1}\left(m_1+1\right)!\left(m_2+1\right)!\left(m_3+1\right)!} \right| A_1 A_2 A_3, \end{aligned} \tag{58}$$

The variables $\prod_{i=0}^{m_1}\left|(x-x_i)\right|$, $\prod_{j=0}^{m_2}\left|(y-y_j)\right|$ and $\prod_{k=0}^{m_3}\left|(t-t_k)\right|$ are changed to derive bounds,

$$\begin{aligned} x &= \theta\frac{R}{m_1}, \\ y &= \phi\frac{N}{m_2}, \\ t &= \varphi\frac{M}{m_3}. \end{aligned} \tag{59}$$

It can be obtained,

$$\begin{aligned} \prod_{i=0}^{m_1}\left|(x-x_i)\right| &= \left(\frac{R}{m_1}\right)^{m_1+1}\prod_{i=0}^{m_1}|\theta-i|, \\ \prod_{j=0}^{m_2}\left|(y-y_j)\right| &= \left(\frac{N}{m_2}\right)^{m_2+1}\prod_{j=0}^{m_2}|\phi-j|, \\ \prod_{k=0}^{m_3}\left|(t-t_k)\right| &= \left(\frac{M}{m_3}\right)^{m_3+1}\prod_{k=0}^{m_3}|\varphi-k|, \end{aligned} \tag{60}$$

where ε_1, ε_2 and ε_3 are proposed as $\varepsilon_1<\theta<\varepsilon_1+1, \varepsilon_2<\phi<\varepsilon_2+1, \varepsilon_3<\varphi<\varepsilon_3+1$.

Following that,

$$\begin{aligned} \prod_{i=0}^{m_1}|\theta-i| &= \left|(\theta-\varepsilon_1)(\theta-\varepsilon_1-1)\right|\prod_{i=0}^{\varepsilon_1-1}|\theta-i|\prod_{i=\varepsilon_1-2}^{m_1}|\theta-i|, \\ \prod_{j=0}^{m_2}|\phi-j| &= \left|(\phi-\varepsilon_2)(\phi-\varepsilon_2-1)\right|\prod_{j=0}^{\varepsilon_2-1}|\phi-j|\prod_{j=\varepsilon_2-2}^{m_2}|\phi-j|, \\ \prod_{k=0}^{m_3}|\varphi-k| &= \left|(\varphi-\varepsilon_3)(\varphi-\varepsilon_3-1)\right|\prod_{k=0}^{\varepsilon_3-1}|\varphi-k|\prod_{k=\varepsilon_3-2}^{m_3}|\varphi-k|, \end{aligned} \tag{61}$$

where $\left|(\theta-\varepsilon_1)(\theta-\varepsilon_1-1)\right|$, $\left|(\phi-\varepsilon_2)(\phi-\varepsilon_2-1)\right|$ and $\left|(\varphi-\varepsilon_3)(\varphi-\varepsilon_3-1)\right|$ at points $\theta+\frac{1}{2}, \phi+\frac{1}{2}$ and $\varphi+\frac{1}{2}$ respectively are their maximum values. Thus,

$$\begin{aligned} \left|(\theta-\varepsilon_1)(\theta-\varepsilon_1-1)\right| &\le \frac{1}{4}, \\ \left|(\phi-\varepsilon_2)(\phi-\varepsilon_2-1)\right| &\le \frac{1}{4}, \\ \left|(\varphi-\varepsilon_3)(\varphi-\varepsilon_3-1)\right| &\le \frac{1}{4}. \end{aligned} \tag{62}$$

Based on Eq. (59), they can be rewritten as follows:

$$\begin{aligned} \prod_{i=0}^{\varepsilon_1-1}|(\theta-i)| &\le \prod_{i=0}^{\varepsilon_1-1}\left|(\varepsilon_1+1-i)\right| \le (\varepsilon_1+1)!, \\ \prod_{j=0}^{\varepsilon_2-1}|(\phi-j)| &\le \prod_{j=0}^{\varepsilon_2-1}\left|(\varepsilon_2+1-j)\right| \le (\varepsilon_2+1)!, \\ \prod_{k=0}^{\varepsilon_3-1}|(\varphi-k)| &\le \prod_{k=0}^{\varepsilon_3-1}\left|(\varepsilon_3+1-k)\right| \le (\varepsilon_3+1)!, \\ \prod_{i=\varepsilon_1-2}^{m_1}|(\theta-i)| &\le \prod_{i=\varepsilon_1-2}^{m_1}\left|(i-\varepsilon_1)\right| \le (m_1-\varepsilon_1)!, \\ \prod_{j=\varepsilon_2-2}^{m_2}|(\phi-j)| &\le \prod_{j=\varepsilon_2-2}^{m_2}\left|(j-\varepsilon_2)\right| \le (m_2-\varepsilon_2)!, \\ \prod_{k=\varepsilon_3-2}^{m_3}|(\varphi-k)| &\le \prod_{k=\varepsilon_3-2}^{m_3}\left|(k-\varepsilon_3)\right| \le (m_3-\varepsilon_3)!. \end{aligned} \tag{63}$$

Combining Eqs. (62) and (63) in Eq. (61), the following bounds are obtained.

$$\begin{aligned} \prod_{i=0}^{m_1}|\theta-i| &\le \frac{1}{4}(m_1+1)!, \\ \prod_{j=0}^{m_2}|\phi-j| &\le \frac{1}{4}(m_2+1)!, \end{aligned}$$

$$\prod_{k=0}^{m_3} |\varphi - k| \le \frac{1}{4}(m_3+1)!. \tag{64}$$

The bounds derived from Eq. (60) are as follows:

$$\begin{aligned}
&\prod_{i=0}^{m_1} \left|(x-x_i)\right| = \left(\frac{R}{m_1}\right)^{m_1+1} \frac{1}{4}(m_1+1)!,\\
&\prod_{j=0}^{m_2} \left|(y-y_j)\right| = \left(\frac{N}{m_2}\right)^{m_2+1} \frac{1}{4}(m_2+1)!,\\
&\prod_{k=0}^{m_3} \left|(t-t_k)\right| = \left(\frac{M}{m_3}\right)^{m_3+1} \frac{1}{4}(m_3+1)!.
\end{aligned} \tag{65}$$

The error bound is found based on Eqs. (58) and (65),

$$\begin{aligned}
&\left|u(x,y,t) - \upsilon_{m_1,m_2,m_3}(x,y,t)\right|\\
&\le \frac{1}{4}\left(\frac{R}{m_1}\right)^{m_1+1} D_1 + \frac{1}{4}\left(\frac{N}{m_2}\right)^{m_2+1} D_2 + \frac{1}{4}\left(\frac{M}{m_3}\right)^{m_3+1} D_3\\
&- \frac{1}{64}\left(\frac{R}{m_1}\right)^{m_1+1}\left(\frac{N}{m_2}\right)^{m_2+1}\left(\frac{M}{m_3}\right)^{m_3+1} D_4,
\end{aligned} \tag{66}$$

where $D_1 = \max_{(x,y,t)\in\Omega}\left|\frac{\partial^{m_1+1}u(x,y,t)}{\partial x^{m_1+1}}\right|$, $D_2 = \max_{(x,y,t)\in\Omega}\left|\frac{\partial^{m_2+1}u(x,y,t)}{\partial y^{m_2+1}}\right|$, $D_3 = \max_{(x,y,t)\in\Omega}\left|\frac{\partial^{m_3+1}u(x,y,t)}{\partial t^{m_3+1}}\right|$ and $D_4 = \max_{(x,y,t)\in\Omega}\left|\frac{\partial^{m_1+m_2+m_3+3}u(x,y,t)}{\partial x^{m_1+1}\partial y^{m_2+1}\partial t^{m_3+1}}\right|$.

Based on Eq. (56), the following error estimation is obtained,

$$\begin{aligned}
&\left\|u(x,y,t) - u_{m_1,m_2,m_3}(x,y,t)\right\|_2\\
&\le \sqrt[3]{RNM}\left(\frac{1}{4}\left(\frac{R}{m_1}\right)^{m_1+1} D_1 + \frac{1}{4}\left(\frac{N}{m_2}\right)^{m_2+1} D_2 + \frac{1}{4}\left(\frac{M}{m_3}\right)^{m_3+1} D_3\right.\\
&\left.-\frac{1}{64}\left(\frac{R}{m_1}\right)^{m_1+1}\left(\frac{N}{m_2}\right)^{m_2+1}\left(\frac{M}{m_3}\right)^{m_3+1} D_4\right).
\end{aligned} \tag{67}$$

4.2. Convergence analysis

The convergence of the SLPs algorithm is ensured by the exponential decay of the error terms in the approximation $u_{m_1,m_2,m_3}(x,y,t)$. As $m_1, m_2, m_3 \to \infty$, the terms $\left(\frac{R}{m_1}\right)^{m_1+1}$, $\left(\frac{N}{m_2}\right)^{m_2+1}$ and $\left(\frac{M}{m_3}\right)^{m_3+1}$ diminish exponentially, ensuring:

$$\left\|u(x,y,t) - u_{m_1,m_2,m_3}(x,y,t)\right\|_2 \to 0, \quad \text{as } m_1, m_2, m_3 \to \infty.$$

The approximation $u_{m_1,m_2,m_3}(x,y,t)$ converges uniformly to $u(x,y,t)$ with an exponential rate governed by the decay of $\left(\frac{R}{m_1}\right)^{m_1+1}$, $\left(\frac{N}{m_2}\right)^{m_2+1}$ and $\left(\frac{M}{m_3}\right)^{m_3+1}$. The convergence highlights the computational efficiency of the SLPs algorithm, and confirms its high effectiveness for approximating ternary functions in VOFPDEs.

4.3. Mathematical example 1

A general mathematical example associated with its analytical solution is proposed. The mathematical example is solved by the proposed SLPs numerical algorithm. The form of the equation is the same as the VOF governing equation of the variable thickness viscoelastic plate with simply supported-clamped boundary conditions, the expression is:

$$0.01 D_t^{\alpha(t)}\left(\frac{\partial^4 u(x,y,t)}{\partial x^4} + 2\frac{\partial^4 u(x,y,t)}{\partial x^2 \partial y^2} + \frac{\partial^4 u(x,y,t)}{\partial y^4}\right) - 0.006\frac{\partial^2 u(x,y,t)}{\partial t^2} = f(x,y,t), \tag{68}$$

where $\alpha(t) = 0.4t + 0.1$, $t \in [0,1]$, $x \in [0,1]$, $y \in [0,1]$.

The initial conditions are:

$$u(x,y,0) = \left.\frac{\partial u(x,y,t)}{\partial t}\right|_{t=0} = 0. \tag{69}$$

The boundary conditions are:

$$u|_{x=0,1} = u|_{y=0,1} = \left.\frac{\partial u}{\partial y}\right|_{y=0,1} = \left.\frac{\partial^2 u}{\partial x^2}\right|_{x=0,1} = 0. \tag{70}$$

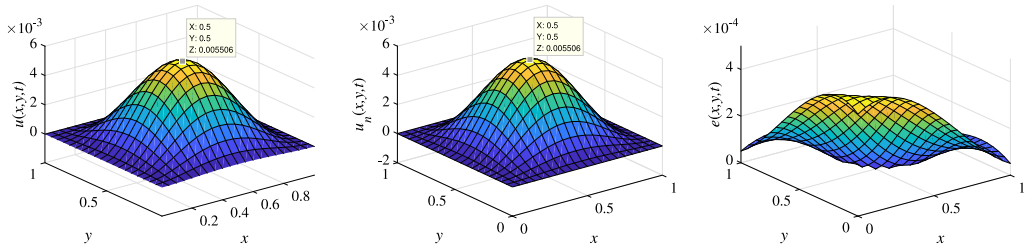

(a) Analytical solution (b) Numerical solution (c) Absolute error

Fig. 3. Numerical analysis of the VOFPDE obtained by SLPs algorithm.

The analytical solution of Eq. (68) is:

$$u(x,y,t) = x^2(1-x)^2 y^2 (1-y)^2 t^2. \tag{71}$$

This equation is solved separately by the SLPs and SBPs algorithms. The numerical solution is represented by $u_n(x,y,t)$. The absolute error is $e(x,y,t) = |u_n(x,y,t) - u(x,y,t)|$, which is presented to show the computational efficiency of the algorithms.

The definition of SBPs on the interval [0,R] is given as [38]:

$$B_{i,n}(x) = \binom{n}{i} \frac{x^i (R-x)^{n-i}}{R^n} = \sum_{k=0}^{n-i} (-1)^k \binom{n-i}{k} \frac{x^{i+k}}{R^{i+k}}, \tag{72}$$

The matrix $\Psi(x)$ consists of a series of SBPs defined over the interval [0,R]. Its formula is given as follows:

$$\Psi(x) = \left[B_{0,n}(x), B_{1,n}(x), \ldots, B_{n,n}(x)\right]^T = BT_n(x), \tag{73}$$

where

$$T_n(x) = \begin{bmatrix} 1 \\ x \\ \vdots \\ x^n \end{bmatrix}, B = \left[b_{i,j}\right]_{i,j=0}^{n}, b_{i,j} = \begin{cases} (-1)^{j-i}\binom{n}{i}\binom{n-i}{j-i}\frac{1}{R^j}, & \text{if } j \geq i, \\ 0, & \text{if } j < i. \end{cases}$$

where B is coefficient matrix of SBPs. It is an upper triangular matrix with non-zero on the main diagonal, so it is invertible. $T_n(x)$ is obtained as:

$$T_n(x) = B^{-1}\Psi(x). \tag{74}$$

The operator matrices of the SBPs are derived to approximate the unknown function by using the same method described in Section 3. These matrices are employed to transform the governing equation into a series of algebraic equations, which are solved subsequently.

The numerical solutions obtained using the algorithms based on SLPs and SBPs, along with their corresponding absolute errors, are shown in Figs. 3 and 4, respectively. As illustrated in Figs. 3(b) and 4(b), both orthogonal polynomials algorithms successfully solve the equation, with the numerical results satisfying the initial and boundary conditions. The accuracy of the two algorithms is compared using absolute error, as shown in Figs. 3(c) and 4(c). The absolute error for the SLPs algorithm is smaller than that of the SBPs algorithm. In terms of computational performance, the SLPs algorithm required 47 s of CPU time, whereas the SBPs algorithm took 68 s. Furthermore, the SLPs algorithm converged after 14 iterations, while the SBPs algorithm required 29 iterations to converge. These results demonstrate that the SLPs algorithm possesses superior computational efficiency and accuracy.

Table 1 presents the values of the absolute and relative errors of the displacements obtained by using the SLPs and SBPs algorithms at various points. This comparison provides a quantitative difference in the numerical accuracy and performance of the algorithms based on these two polynomials. It is evident that SLPs outperform SBPs in both absolute and relative errors at all the selected points. The algorithm based on SLPs demonstrates significantly lower absolute errors, with values ranging from 1.521×10^{-8} to 1.182×10^{-4}, compared to the algorithm based on SBPs, with the values ranging from 8.560×10^{-4} to 1.007×10^{-3}. The relative error for SLPs is consistently below 2.528×10^{-2} %, while SBPs exhibit a higher relative error of 1.830×10^{-1} %. These findings confirm the accuracy and reliability of SLPs algorithm in the approximation of solution of the fractional governing equation.

4.4. Mathematical example 2

The following mathematical example is studied to further validate the applicability of the SLPs algorithm to VOFPDEs with diverse boundary conditions and fractional derivatives.

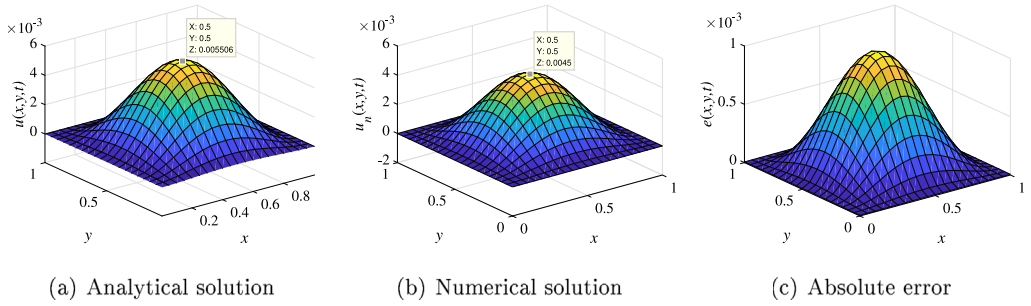

Fig. 4. Numerical analysis of the VOFPDE obtained by SBPs algorithm.

Table 1
Error comparison between the algorithms based on SLPs and SBPs at various points.

(x, y)	Absolute error		Relative error (%)	
	SLPs	SBPs	SLPs	SBPs
(0.4, 0.4)	1.182×10^{-4}	8.560×10^{-4}	2.528×10^{-2}	1.830×10^{-1}
(0.5, 0.4)	5.713×10^{-5}	9.282×10^{-4}	1.113×10^{-2}	1.829×10^{-1}
(0.6, 0.4)	2.126×10^{-5}	8.560×10^{-4}	4.547×10^{-3}	1.830×10^{-1}
(0.4, 0.5)	5.713×10^{-5}	9.282×10^{-4}	1.113×10^{-2}	1.829×10^{-1}
(0.5, 0.5)	1.521×10^{-8}	1.007×10^{-3}	2.762×10^{-6}	1.828×10^{-1}
(0.6, 0.5)	2.908×10^{-5}	9.282×10^{-4}	5.731×10^{-3}	1.829×10^{-1}
(0.4, 0.6)	2.126×10^{-5}	8.560×10^{-4}	4.547×10^{-3}	1.830×10^{-1}
(0.5, 0.6)	2.908×10^{-5}	9.282×10^{-4}	5.731×10^{-3}	1.829×10^{-1}
(0.6, 0.6)	5.360×10^{-5}	8.560×10^{-4}	1.146×10^{-2}	1.830×10^{-1}

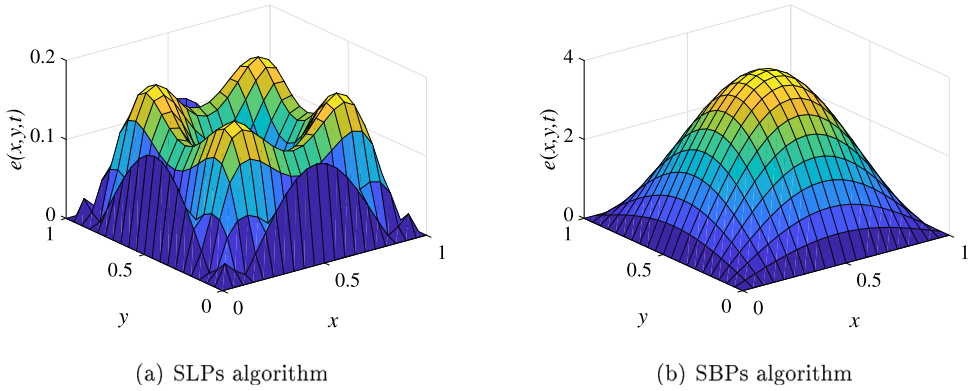

Fig. 5. Absolute error obtained by using the SLPs and SBPs algorithms.

$$0.03 D_t^{\alpha(t)} \left(\frac{\partial^4 u(x,y,t)}{\partial x^4} + 2\frac{\partial^4 u(x,y,t)}{\partial x^2 \partial y^2} + \frac{\partial^4 u(x,y,t)}{\partial y^4} \right) + 100 \frac{\partial^2 u(x,y,t)}{\partial t^2} = f(x,y,t), \tag{75}$$

where $\alpha(t) = 0.1t + 0.5$, $t \in [0,1]$, $x \in [0,1]$, $y \in [0,1]$.

The initial conditions are:

$$u(x,y,0) = \left. \frac{\partial u(x,y,t)}{\partial t} \right|_{t=0} = 0. \tag{76}$$

The boundary conditions are:

$$u|_{x=0,1} = u|_{y=0,1} = \left. \frac{\partial^2 u}{\partial y^2} \right|_{y=0,1} = \left. \frac{\partial^2 u}{\partial x^2} \right|_{x=0,1} = 0. \tag{77}$$

The analytical solution of Eq. (75) is in the form of a harmonic function:

$$u(x,y,t) = 5\sin(\pi x)\sin(\pi y)t^2. \tag{78}$$

Table 2
Material parameters of the model [38].

Material	ρ (kg/m^3)	θ (s)	E (Pa)	ν	$\alpha(t)$
PET	1380	0.35	3×10^7	0.3	$-0.1t+1$
Polyurea	1060	0.0012	1.2×10^7	0.3	$-0.1t+1$

This equation is solved by using the SLPs and SBPs algorithms. A comparison of the absolute errors, presented in Fig. 5, indicates that the SLPs algorithm is more accurate than the SBPs algorithm. The computation time for the SLPs algorithm is 6.5 s of CPU time, compared to 9.5 s for the SBPs algorithm. Additionally, the SLPs algorithm converged after 23 iterations, whereas the SBPs algorithm required 95 iterations to achieve convergence. These results demonstrate that the SLPs algorithm can approximate more complex analytical solutions with significantly reduced convergence rate.

The stability of the algorithm based on SLPs is validated by the obtained absolute and relative errors for solving the VOFPDEs with the various fractional derivatives under different boundary conditions.

5. Numerical investigation of variable thickness viscoelastic plates

SLPs algorithm is used to solve the governing equations of viscoelastic plates with variable thickness. The evolution of displacement of plates with varying thicknesses and materials under the harmonic load is analysed. The displacement, stress and bending moment of quadratic variable thickness PET plate are studied.

The boundary conditions of the plate with $a = 3$ m and $b = 2$ m are:

$$u|_{x=0,3} = u|_{y=0,2} = \left.\frac{\partial u}{\partial y}\right|_{y=0,2} = \left.\frac{\partial^2 u}{\partial x^2}\right|_{x=0,3} = 0. \tag{79}$$

Thickness variations of the plate are represented by three different distribution functions as:

$$\begin{aligned}
&\textit{Linear thickness variation}: h(y) = h_0\left[1+\lambda\left(\frac{2y}{b}-1\right)\right],\\
&\textit{Quadratic thickness variation}: h(y) = h_0\left[1+\lambda\left(\frac{2y}{b}-1\right)^2\right],\\
&\textit{Cubic thickness variation}: h(y) = h_0\left[1+\lambda\left(\frac{2y}{b}-1\right)^3\right],
\end{aligned} \tag{80}$$

where $h_0 = 0.01$ m, $\lambda = 0.1$.

5.1. Numerical analysis of plates with different materials and thicknesses

The materials used for the variable thickness viscoelastic plates are PET and polyurea. Table 2 summarizes the material parameters utilized in the VOF model.

The displacement variations of PET and polyurea plates with linear, quadratic and cubic thickness changes under harmonic load $F = F_0 \sin(\pi x/a)\sin(\pi y/b)\cos(\omega t)$ [39] are analysed, where F_0 is amplitude and ω is excitation frequency. Substituting $F_0 = 0.015$ N/m, $\omega = 0.7$ rad/s, $t = 2$ s and $\alpha(t) = -0.1t + 1$ into Eq. (15), the displacement solution is obtained in the time domain. As shown in Figs. 6 and 7, the maximum displacement occurs at the centre position of the plate $(x, y) = (1.5, 1)$. The displacements at the four edges of the plate are equal to 0, satisfying the boundary conditions. Among plates made from the same material, the plate with a linear thickness variation exhibits the largest displacement, while the plate with a quadratic thickness variation shows the smallest displacement. The results were coherent with those presented in Zenkour's study [40], where the numerical results for variable thickness rectangular plates under different boundary conditions were provided. In this study, the numerical results are represented by using the two-dimensional graphics, offering a clear and direct representation of the numerical data. The effectiveness of the algorithm based on SLPs in solving the governing equations for variable thickness plates is demonstrated.

As shown in Fig. 8, the displacement solutions of the PET and polyurea plates at $y = 1$ m are obtained in the time domain for various values of x. The results indicate that the displacement is smaller in PET than in polyurea plates, demonstrating that PET plates are more resistant to bending. The findings of this study align with the investigations of PET and polyurea rotating beam, reported in [38]. These results confirmed that the VOF model could effectively describe the viscoelastic characteristics, providing a robust theoretical foundation for the performance prediction of damping materials. PET plates with quadratic thickness variations exhibit small displacement, which is ideal for the applications requiring high stiffness, such as structural components in aerospace and automotive industries. Polyurea is well-suited for the applications involving vibration and shock absorption.

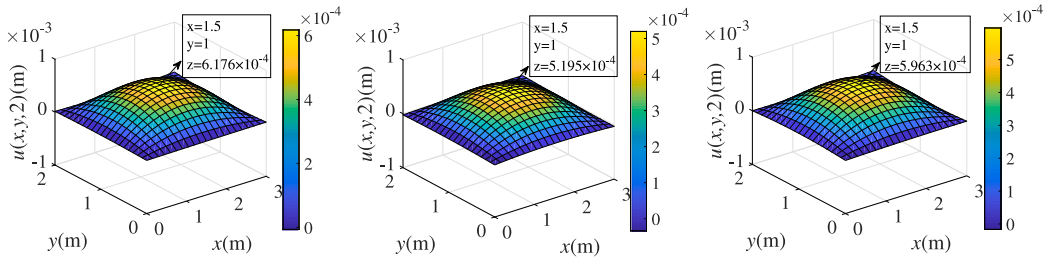

(a) *Linear thickness variation* (b) *Quadratic thickness variation* (c) *Cubic thickness variation*

Fig. 6. Displacement solutions of three thickness variations of PET plates.

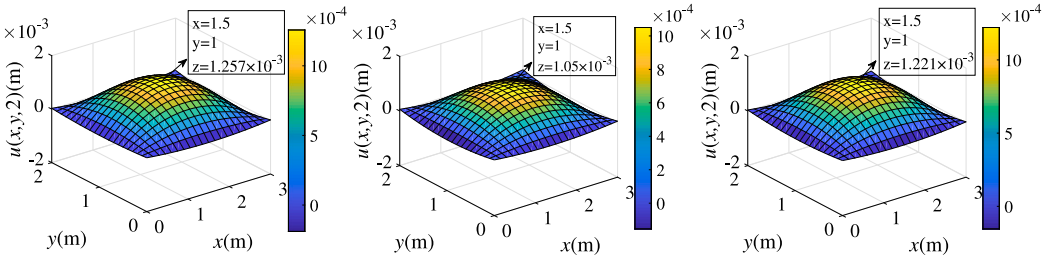

(a) *Linear thickness variation* (b) *Quadratic thickness variation* (c) *Cubic thickness variation*

Fig. 7. Displacement solutions of three thickness variations of polyurea plates.

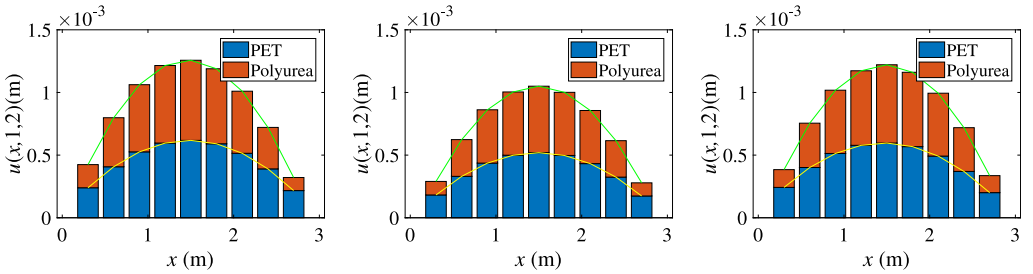

(a) *Linear thickness variation* (b) *Quadratic thickness variation* (c) *Cubic thickness variation*

Fig. 8. Comparison of displacement solutions of the PET plate and polyurea plate under three thickness variations.

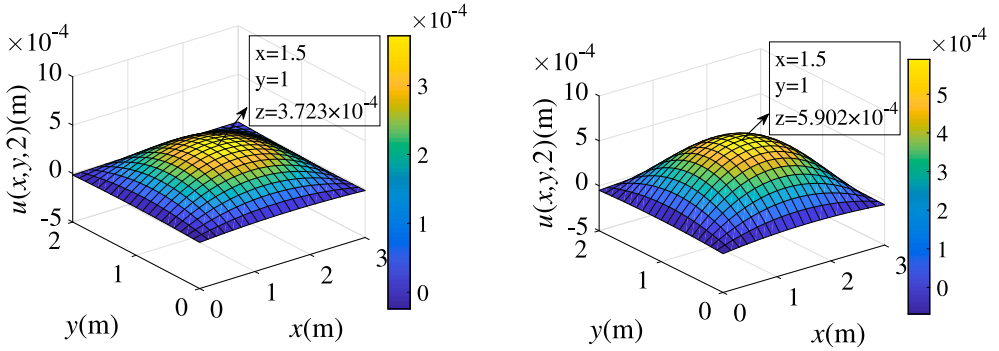

(a) $F = 0.01\sin\left(\frac{\pi x}{3}\right)\sin\left(\frac{\pi y}{2}\right)\cos(0.7t)$ (b) $F = 0.02\sin\left(\frac{\pi x}{3}\right)\sin\left(\frac{\pi y}{2}\right)\cos(0.7t)$

Fig. 9. Displacement solutions of PET plate under different amplitudes.

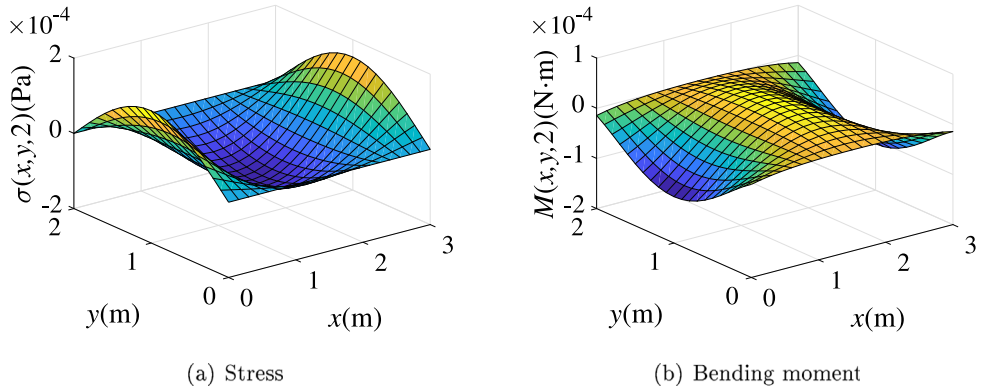

Fig. 10. 2D distribution of stress and bending moment of quadratic variable thickness rectangular plate in x–y plane.

5.2. Effect of the amplitude of harmonic load

When $F_0 = 0.01$ N/m and $F_0 = 0.02$ N/m in harmonic load, the displacement of the quadratic variable thickness PET plate is calculated, as shown in Fig. 9. The results indicate that the displacement increases progressively with F_0.

When $F_0 = 0.015$ N/m, the numerical solutions of the stress and bending moment of the plate are illustrated in Fig. 10. In Fig. 10(a), the stress is shown to disappear at $y = 0$ m and $y = 2$ m, while its maximum value occurs at $x = 0$ m and $x = 3$ m when $y = 1$ m. The minimum value of stress occurs at the centre of the plane. As depicted in Fig. 10(b), the maximum bending moment appears at the centre of the plate, while the minimum bending moment is observed at $x = 0$ m and $x = 3$ m when $y = 1$ m. The bending moment almost disappears at $y = 0$ m and $y = 2$ m. The results obtained in this study are consistent with those presented in [41]. Zenkour employed the small parameter and Lévy-type methods to obtain the dimensionless displacement. This study provides the numerical results directly in the time domain, offering a practical perspective for designers of variable thickness structures.

6. Conclusions

In this paper, an innovative algorithm based on SLPs is proposed for solving the governing equation of variable thickness viscoelastic plates. The VOF model effectively describes the relationship between stress and strain in the plate. Displacement, stress and bending moment are analysed in the time domain. The key conclusions are summarized as follows:

1. VOF model with linear order function is successfully implemented in the governing equation of viscoelastic plate with the advantages of high efficiency and accuracy.
2. The VOFPDEs of variable thickness viscoelastic plates are directly solved in the time domain by using SLPs algorithm.
3. Comparing to SBPs, the SLPs algorithm exhibits superior accuracy, faster convergence rate and reduced computational time.
4. Viscoelastic plate with quadratic thickness variation exhibits the smallest displacement change under the same loading conditions.
5. PET demonstrates better bending performance than polyurea, making it more suitable for applications requiring high stiffness.
6. The displacement of the plate gradually increases with the amplitude of the uniformly distributed harmonic load.

The material studied in this research is incompressible and isotropic, which simplifies the modelling process, but limits its applicability to compressible or anisotropic materials. The instability and convergence issues of the numerical method appear under extreme conditions, such as when the diffusion rate approaches zero. It can reduce accuracy and increase computational cost. These limitations highlight the need for further advancements in modelling and computational techniques. Future research will focus on the extension of the fractional viscoelastic models to multi-scale and multi-physics problems to enhance the accuracy of behaviour predictions for complex materials, with specific applications to additive manufacturing (3D printing) process. The effects of thermal, mechanical, and viscoelastic interactions will be thoroughly explored by employing FO models in a multi-physics framework. The physical significance of VOF derivatives will be investigated to provide a deeper understanding of their role in describing complex material behaviour. A fractional derivative UMAT (User Material) subroutine is being developed for the integration with finite element method. This tool will enable more precise investigations of viscoelastic behaviour under diverse conditions and configurations, facilitate the significant advancements in the application of VOF models in engineering and material science.

CRediT authorship contribution statement

Lin Sun: Writing – original draft, Software, Writing – review & editing. **Jingguo Qu:** Writing – review & editing. **Gang Cheng:** Writing – review & editing, Supervision. **Thierry Barrière:** Writing – review & editing. **Yuhuan Cui:** Writing – review & editing. **Aimin Yang:** Funding acquisition. **Yiming Chen:** Formal analysis.

Declaration of competing interest

The authors declare that they have no known competing financial interests or personal relationships that could have appeared to influence the work reported in this paper.

Acknowledgements

This work is supported by China Scholarship Council (No. 2022018130033), National Natural Science Foundation of China (No. 5207041692) and Hebei Outstanding Youth Fund Project (E2020209082).

Data availability

No data was used for the research described in the article.

References

[1] Wang C, Yao G. Nonlinear dynamics of variable thickness plates interacting with subsonic flow. J Vib Eng Technol 2024;12:5411–22. http://dx.doi.org/10.1007/s42417-023-01171-5.
[2] Gupta A, Khanna A. Vibration of clamped visco-elastic rectangular plate with parabolic thickness variations. Shock Vib 2008;15:713–23. http://dx.doi.org/10.1155/2008/873049.
[3] Gupta A, Kaur H, Kumar S. Thermal effect on vibration of clamped visco-elastic rectangular plate with parabolic thickness variation in both directions. Shock Vib 2010;17:93–105. http://dx.doi.org/10.3233/SAV-2010-0500.
[4] Yu Q. A homotopy-based wavelet method for extreme large bending analysis of heterogeneous anisotropic plate with variable thickness on orthotropic foundation. Appl Math Comput 2023;439:127641. http://dx.doi.org/10.1016/j.amc.2022.127641.
[5] Alipour M, Shariyat M. Semi-analytical buckling analysis of heterogeneous variable thickness viscoelastic circular plates on elastic foundations. Mech Res Commun 2011;38:594–601. http://dx.doi.org/10.1016/j.mechrescom.2011.09.001.
[6] Sun H, Zhang Y, Baleanu D, Chen W, Chen Y. A new collection of real world applications of fractional calculus in science and engineering. Commun Nonlinear Sci Numer Simul 2018;64:213–31. http://dx.doi.org/10.1016/j.cnsns.2018.04.019.
[7] Yu Y, Perdikaris P, Karniadakis G. Fractional modeling of viscoelasticity in 3D cerebral arteries and aneurysms. J Comput Phys 2016;323:219–42. http://dx.doi.org/10.1016/j.jcp.2016.06.038.
[8] Qing J, Zhou S, Wu J, Shao M. Nonlinear dynamics of fractional viscoelastic PET membranes with linearly varying density. Commun Nonlinear Sci Numer Simul 2023;127:107559. http://dx.doi.org/10.1016/j.cnsns.2023.107559.
[9] Zhang J, Fang Z, Sun H. Robust fast method for variable-order time-fractional diffusion equations without regularity assumptions of the true solutions. Appl Math Comput 2022;430:127273. http://dx.doi.org/10.1016/j.amc.2022.127273.
[10] Gao Y, Yin D, Zhao B. A variable-order fractional constitutive model to characterize the rate-dependent mechanical behaviour of soft materials. Fractal Fract 2022;6:590. http://dx.doi.org/10.3390/fractalfract6100590.
[11] Meng R, Cao L, Zhang Q. Study on the performance of variable-order fractional viscoelastic models to the order function parameters. Appl Math Model 2023;121:430–44. http://dx.doi.org/10.1016/j.apm.2023.05.017.
[12] Sun L, Cheng G, Barriere T. Investigation of temperature-dependent mechanical behaviours of polycarbonate with an innovative fractional order model. Mater Res Proc 2024;41:2174–81. http://dx.doi.org/10.21741/9781644903131-239.
[13] Sun L, Chen Y. Numerical analysis of variable fractional viscoelastic column based on two-dimensional Legendre wavelets algorithm. Chaos Solitons Fractals 2021;152:111372. http://dx.doi.org/10.1016/j.chaos.2021.111372.
[14] Hassani H, Tenreiro Machado J, Naraghirad E. An efficient numerical technique for variable order time fractional nonlinear Klein–Gordon equation. Appl Numer Math 2020;154:260–72. http://dx.doi.org/10.1016/j.apnum.2020.04.001.
[15] Hassani H, Naraghirad E. A new computational method based on optimization scheme for solving variable-order time fractional Burgers' equation. Math Comput Simulation 2019;162:1–17. http://dx.doi.org/10.1016/j.matcom.2019.01.002.
[16] Dahaghin M, Hassani H. An optimization method based on the generalized polynomials for nonlinear variable-order time fractional diffusion-wave equation. Nonlinear Dynam 2017;88:1587–98. http://dx.doi.org/10.1007/s11071-017-3330-7.
[17] Hosseininia M, Heydari M, Avazzadeh Z. Orthonormal shifted discrete Legendre polynomials for the variable-order fractional extended Fisher-Kolmogorov equation. Chaos Solitons Fractals 2022;155:111729. http://dx.doi.org/10.1016/j.chaos.2021.111729.
[18] Hosseininia M, Heydari M, Avazzadeh Z, Ghaini F. A hybrid method based on the orthogonal Bernoulli polynomials and radial basis functions for variable order fractional reaction-advection-diffusion equation. Eng Anal Bound Elem 2021;127:18–28. http://dx.doi.org/10.1016/j.enganabound.2021.03.006.
[19] Zhao T, Zhao L. Jacobian spectral collocation method for spatio-temporal coupled Fokker–Planck equation with variable-order fractional derivative. Commun Nonlinear Sci Numer Simul 2023;124:107305. http://dx.doi.org/10.1016/j.cnsns.2023.107305.
[20] Hassani H, Tenreiro Machado J, Avazzadeh Z, Naraghirad E. Generalized shifted Chebyshev polynomials: Solving a general class of nonlinear variable order fractional PDE. Commun Nonlinear Sci Numer Simul 2020;85:105229. http://dx.doi.org/10.1016/j.cnsns.2020.105229.
[21] Hassani H, Avazzadeh Z, Tenreiro Machado J. Numerical approach for solving variable-order space–time fractional telegraph equation using transcendental Bernstein series. Eng Comput 2020;36:567–878. http://dx.doi.org/10.1007/s00366-019-00736-x.
[22] Hassani H, Avazzadeh Z, Agarwal P, Ebadi M, Eshkaftaki A. Generalized Bernoulli–Laguerre polynomials: Applications in coupled nonlinear system of variable-order fractional PDEs. J Optim Theory Appl 2024;200:371–93. http://dx.doi.org/10.1007/s10957-023-02346-6.
[23] Mahmoud A, Mohra Z, Ali Y, Manuel S. On conformable fractional Legendre polynomials and their convergence properties with applications. Alex Eng J 2020;59:5231–45. http://dx.doi.org/10.1016/j.aej.2020.09.052.
[24] Heydari M, Atangana A, Avazzadeh Z. Numerical solution of nonlinear fractal-fractional optimal control problems by Legendre polynomials. Appl Math Lett 2020;107:106443. http://dx.doi.org/10.1016/j.aml.2020.106443.
[25] Singh H, Fhassabzadeh F, Tohidi E, Cattani C. Legendre spectral method for the fractional Bratu problem. Math Methods Appl Sci 2020;43:5941–52. http://dx.doi.org/10.1002/mma.6326.
[26] Xie Y, Li L, Wang M. Adomian decomposition method with orthogonal polynomials: Laguerre polynomials and the second kind of Chebyshev polynomials. Mathematics 2021;9:1796. http://dx.doi.org/10.3390/math9151796.
[27] Cao J, Chen Y, Wang Y, Cheng G, Barrière T. Shifted Legendre polynomials algorithm used for the dynamic analysis of PMMA viscoelastic beam with an improved fractional model. Chaos Solitons Fractals 2020;141:110342. http://dx.doi.org/10.1016/j.chaos.2020.110342.

[28] Sun L, Chen Y, Dang R, Cheng G, Xie J. Shifted Legendre polynomials algorithm used for the numerical analysis of viscoelastic plate with a fractional order model. Math Comput Simulation 2022;193:190–203. http://dx.doi.org/10.1016/j.matcom.2021.10.007.
[29] Smit W, Vries H. Rheological models containing fractional derivatives. Rheol Acta 1970;9:525–34. http://dx.doi.org/10.1007/BF01985463.
[30] Meng R, Yin D, Drapaca C. Variable-order fractional description of compression deformation of amorphous glassy polymers. Comput Mech 2019;64:163–71. http://dx.doi.org/10.1007/s00466-018-1663-9.
[31] Coimbra C. Mechanics with variable-order differential operators. Ann Phys 2003;12:692–703. http://dx.doi.org/10.1002/andp.200310032.
[32] Xiang G, Yin D, Meng R, Cao C. Predictive model for stress relaxation behavior of glassy polymers based on variable-order fractional calculus. Polym Adv Technol 2021;32:703–13. http://dx.doi.org/10.1002/pat.5123.
[33] Sitharam T, Govindaraju L. Stress–strain relations. In: Theory of elasticity. Singapore: Springer; 2021, http://dx.doi.org/10.1007/978-981-33-4650-5_4.
[34] Rouzegar J, Vazirzadeh M, Heydari M. A fractional viscoelastic model for vibrational analysis of thin plate excited by supports movement. Mech Res Commun 2020;110:103618. http://dx.doi.org/10.1016/j.mechrescom.2020.103618.
[35] Bhrawy A, Al-Shomrani M. A shifted Legendre spectral method for fractional-order multi-point boundary value problems. Adv Differ Equ 2012;1:8. http://dx.doi.org/10.1186/1687-1847-2012-8.
[36] Li Y, Jiang Y, Yang P. Model order reduction of port-Hamiltonian systems with inhomogeneous initial conditions via approximate finite-time gramians. Appl Math Comput 2022;422:126959. http://dx.doi.org/10.1016/j.amc.2022.126959.
[37] Atkinson K, Han W, Stewart D. Numerical solution of ordinary differential equations. Wiley; 2009.
[38] Han C, Chen Y, Liu D, Driss B. Numerical analysis of viscoelastic rotating beam with variable fractional order model using shifted Bernstein-Legendre polynomial collocation algorithm. Fractal Fract 2021;5:8. http://dx.doi.org/10.3390/fractalfract5010008.
[39] Tuwa P, Miwadinou C, Monwanou A, Orou J, Woafo P. Chaotic vibrations of nonlinear viscoelastic plate with fractional derivative model and subjected to parametric and external excitations. Mech Res Commun 2019;97:8–15. http://dx.doi.org/10.1016/j.mechrescom.2019.04.001.
[40] Zenkour M. An exact solution for the bendingof thin rectangular plates with uniform, linear, and quadratic thickness variations. Int J Mech Sci 2003;45:295–315. http://dx.doi.org/10.1016/S0020-7403(03)00050-X.
[41] Zenkour A, Ashraf M. Bending of thin rectangular plates with variable-thickness in a hygrothermal environment. Thin Wall Struct 2018;123:333–40. http://dx.doi.org/10.1016/j.tws.2017.11.038.